Matter, Volume *3*

Supplemental Information

On-Mask Chemical Modulation of Respiratory Droplets

Haiyue Huang, Hun Park, Yihan Liu, and Jiaxing Huang

Supplemental Data

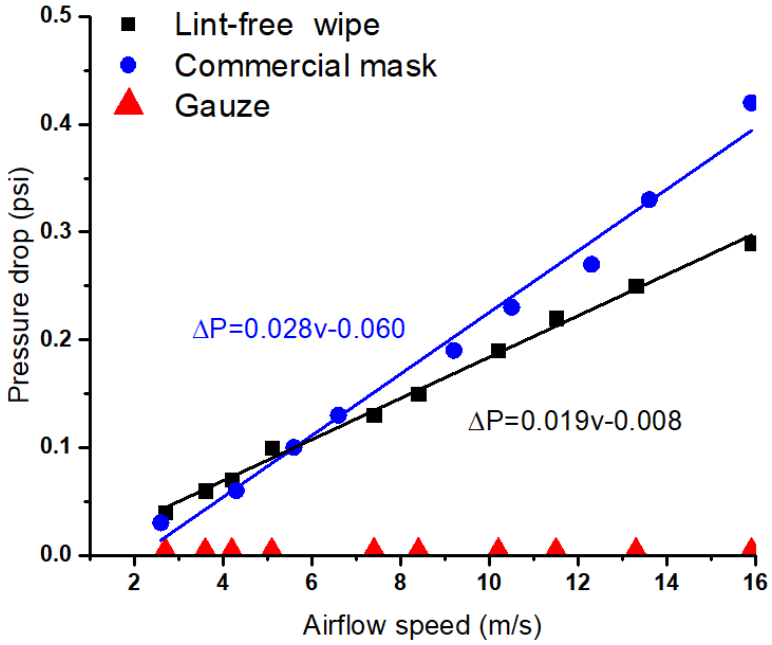

Fig. S1 Pressure drop across different fabrics at different airflow speeds. The pressure drop of gauze was below the measuring limit. The commercial mask sample refers to a typical medical mask with a dense middle layer of melt-spun polypropylene fiber mat.

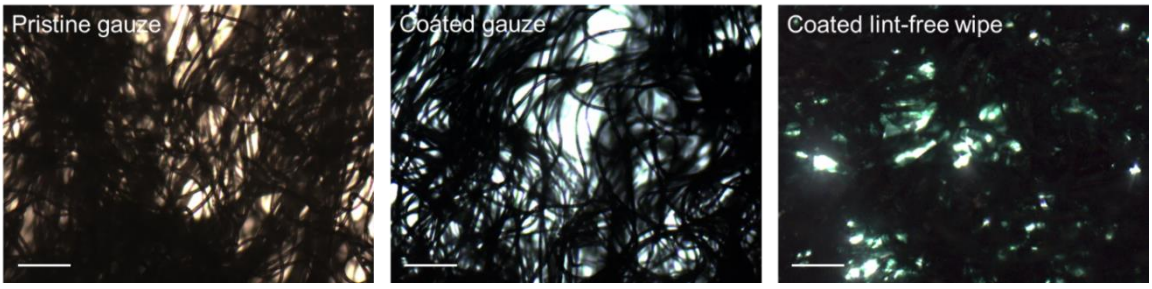

Fig. S2 Optical microscopic images under transmission mode for a pristine gauze (left), a coated gauze (middle), and a coated lint-free wipe (right), respectively. The gauze is less densely packed compared to the lint-free wipe. Scale bars are 200 μm.

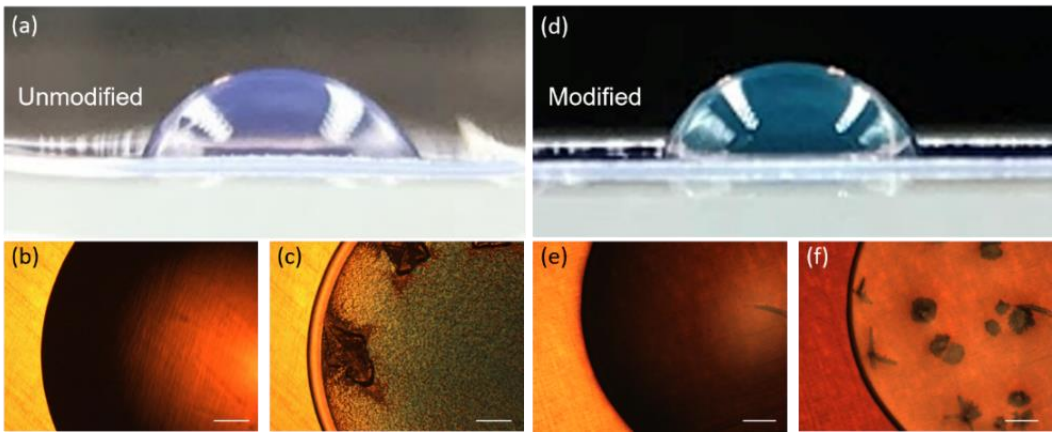

Fig. S3 Observation of contact angle and contact line of droplets on polyaniline detector film. Side view of a 10-μL droplet of (a) unmodified and (d) modified model fluid on polyaniline coated detector film, showing similar contact angles. Top view of 2 μL of unmodified droplet, (b) before and (c) after drying, showing that the initial contact line becomes the edge of the final dried stain. (e-f) This is also observed for an acid modified droplet. All scale bars are 200 μm.

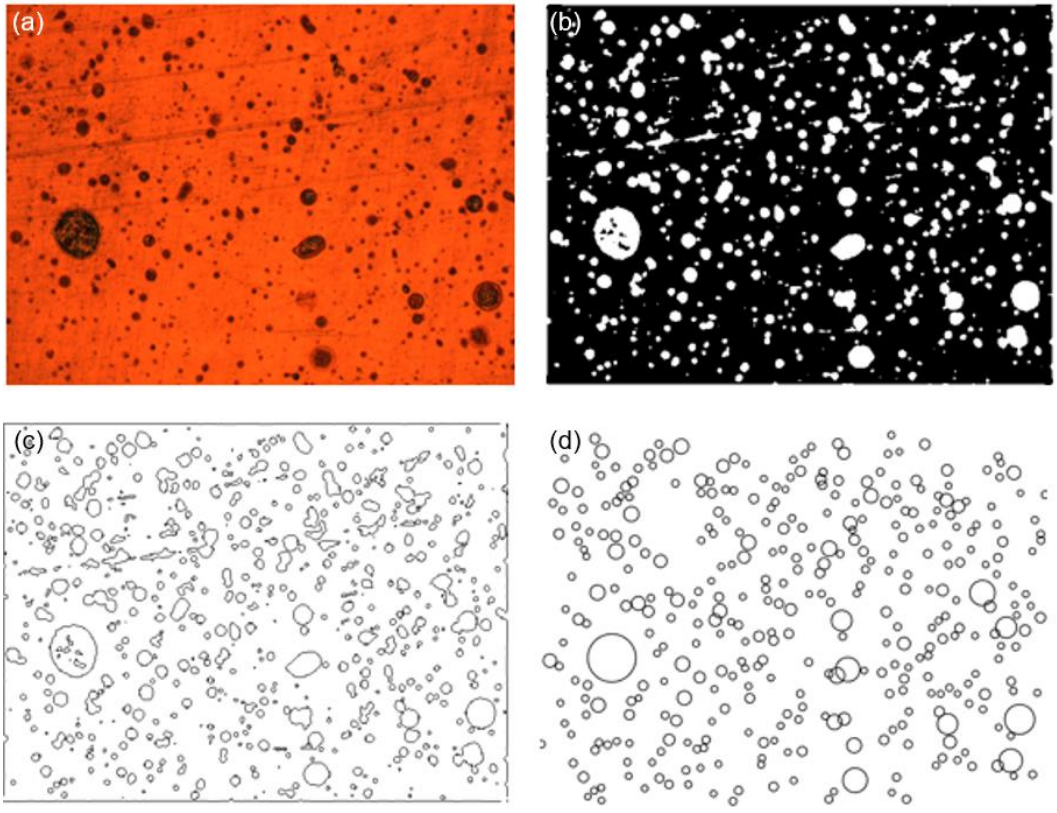

Fig. S4 Hough circle transformation removes unwanted features from (a) the raw image taken under reflection mode, such as the lines of rolling mark on the plastic film. (b) Pre-processing steps are then performed to convert it to a binarized image with reduced noise and inversed contrast. (c) If directly converted to outlines, artifacts associated with the rolling mark are also included. (d) With Hough circle transformation, droplets are approximated as circles and those high-aspect-ratio artifacts are removed, improving the overall accuracy of recognizing droplets.

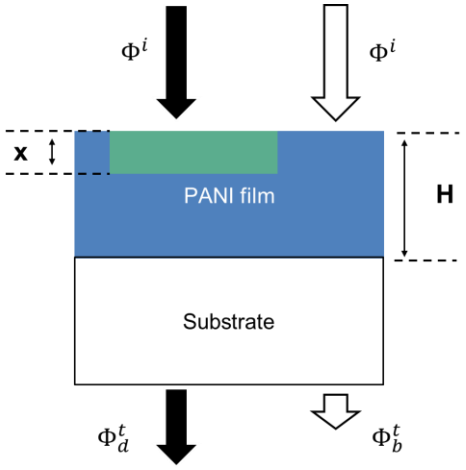

Fig. S5 Parameters used to calculate contrast in transmission images. The doped range of polyaniline (*i.e.*, stain of a modified droplet) was approximated as a cylinder with thickness of *x*. The total thickness of the polyaniline layer is *H*. Φ^i is the intensity of incident light, Φ^t_d is the intensity of transmitted light for a pixel inside a droplet, Φ^t_b is the intensity of transmitted light for a pixel belonging to the background.

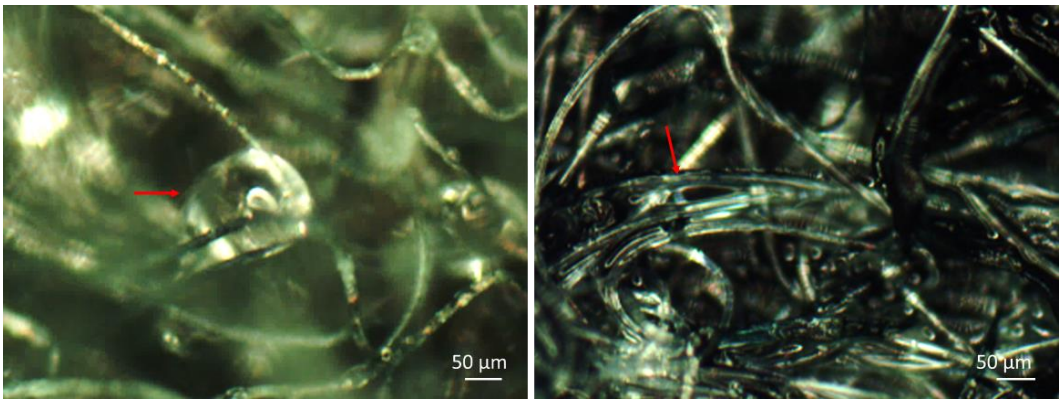

Fig. S6 Optical microscopy images (reflective mode, dark field) of a polyaniline-coated gauze (left) and wipe (right) immediately after spraying. As indicated by the red arrows, large droplets and even liquid films can be observed trapped between fibers.

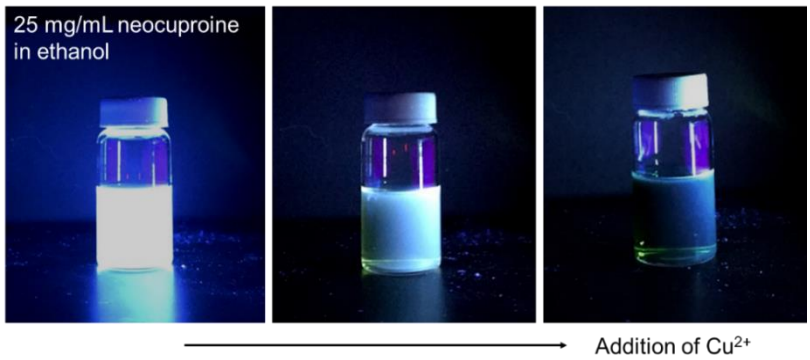

Fig. S7 Quenching of neocuproine's (Nc) fluorescence by Cu^{2+}. The fluorescence of Nc was excited by a UV lamp placed outside the image, which irradiated the sample from the right side. With the addition of $CuSO_4$, the fluorescence was clearly quenched. This inspires the use of Nc dye in fluorescence quenching microscopy to image Cu-modified droplets.

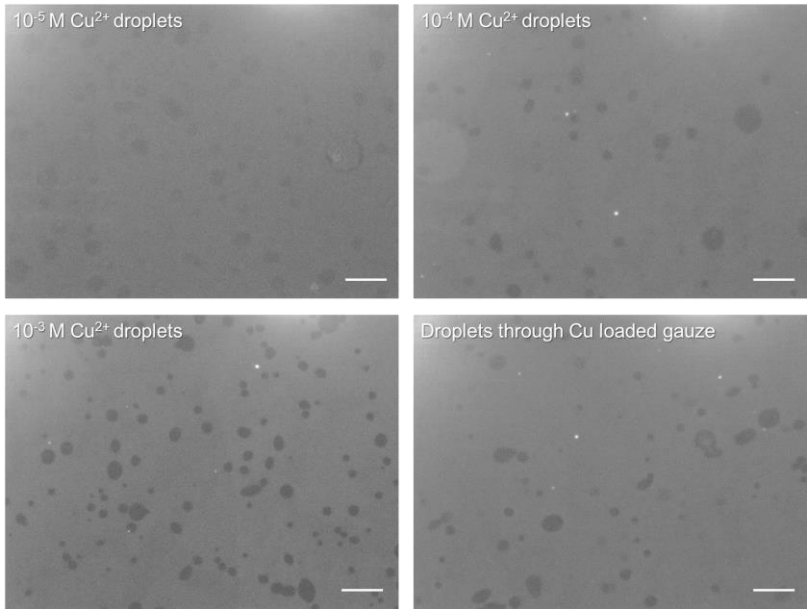

Fig. S8 Fluorescence quenching microscopic images for drying stains of droplets with different concentrations of Cu^{2+}. Model respiratory fluid with different concentrations of Cu^{2+} (10^{-5} to 10^{-3} M) were sprayed to the fluorometric detector films. Stains of the droplets start to show clear contrast against the background when the Cu concentration is larger than 10^{-4} M. An image for droplets passing through a Cu-loaded gauze is also included (obtained under the same condition as **Fig. 10e**), indicating modified droplets have a Cu concentration of at least $>10^{-4}$ M. All scale bars are 50 μm.

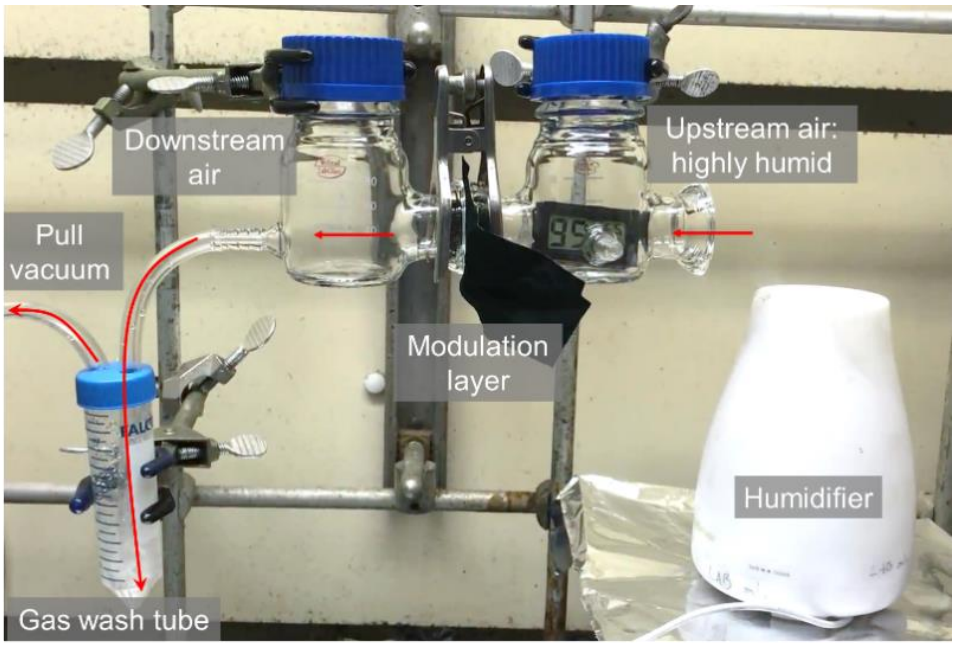

Fig. S9 Experimental setup to simulate inhalation of humid air through a damp fabric. An ultrasonic humidifier was used to generate 99% relative humidity (RH) in the upstream air (measured by a sensor inside the upstream chamber), which was drawn through the lint-free wipe loaded with copper ions or acids. The wipe was sandwiched between two chambers, one of which was connected to the house vacuum. The downstream air was then guided to a tube and bubbled through 10 mL of deionized water reservoir to dissolve released copper ions or acids, if any. No condensation of water was observed in the downstream chamber for all these flow rates. A valve (not shown) was used to control the airflow rate.

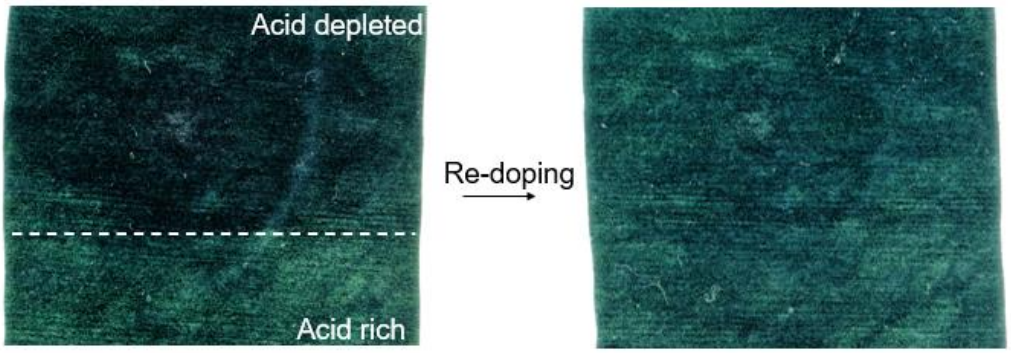

Fig. S10 Acid-depleted area of the polyaniline-coated gauze appears darker than the acid-rich area, giving a visual indicator for replacement or reloading acid (or copper ions).

Table S1. Experimental conditions used in this work in comparison to real expiratory human activities. Data were adapted from references[1-3].

	Sneezing	Coughing	Our experiment
Airflow speed	Up to 30-100 m/s		20 m/s
Droplet speed	~20 m/s	~10 m/s	
Time duration	~0.3-0.7 s		1 s
Droplet concentration	~10^4 droplets or more per sneeze	~10^2-10^3 or more per cough	12 μL/s
Droplet diameter	10-1,000 μm		10-160 μm

Table S2. Number of images and droplets analyzed for **Fig. 8** in the main text.

Sample	Number of images	Number of droplets
Control	13	5,167
Gauze	51	16,688
Lint-free wipe	58	4,524

Table S3 Concentrations of modifiers (acids and copper ions) detected in the 10-mL water reservoir (**Fig. S9**) after simulated inhalation tests in 99% RH through damp wipes.

Experimental condition	Concentration of modifiers in reservoir		"Inhalation" dosage of Cu (mass/volume of "inhaled" air) *
	pH	Cu	
Unmodified wipe, 6 m/s for 10 min	6.97	1.54 ppb	9.58×10^{-10} μg/cm^3
0.2 m/s for 1 h	5.62	2.52 ppb	7.87×10^{-9} μg/cm^3
1 m/s for 1 h	5.62	3.96 ppb	2.47×10^{-9} μg/cm^3
6 m/s for 10 min	5.06	53.23 ppb	3.32×10^{-8} μg/cm^3

* Inhalation dosage (μg/cm^3) was calculated by dividing the amount of detected copper ion (μg) by the product of airflow speed (m/s), duration of the flow (s) and the cross-sectional area of the gas tube (0.28 cm^2). In comparison, the mean copper concentration in natural water is around 60-150 ppb, and the upper limit of Cu level in drinkable water is 20 ppm.[4] Recommended dietary Cu allowance is around 500 μg.[5]

Table S4. Information of lint-free wipes and gauzes.

	Composition	Thickness (mm)	Packing density
Lint-free wipe	45% cellulose/ 55% polyester	0.29 ± 0.03	19%
Gauze	Polyester	0.36 ± 0.06	11%

Supplemental Experimental Procedures

Materials and parameters. Table S1 compares the parameters for coughing and sneezing with our experimental conditions. The airflow speed was measured by pointing a hot wire anemometer (Fishier Brand Traceable) next to the sprayer when it was not filled with any liquid. When filled with liquid, the flux of liquid ejection was measured by spraying the liquid to a container for 10 seconds and measuring the mass of the received liquid. As shown by the table, the experimental condition is comparable to that of coughing and sneezing.

To test if the substrate fabric is breathable enough, the pressure drop (pressure difference between the upstream and downstream) was measured at different airflow speeds. The fabrics to be measured were clamped between two chambers with a hot wire anemometer inserted in the downstream chamber to measure the airflow speeds. A manometer (Control Company #3461) was employed to obtain pressure difference between the upstream and downstream chambers. A lint-free wipe, a gauze, and a commercial mask (VWR maximum protection mask, VWR north America #414004-670) were tested. The result in **Fig. S1** indicates the lint-free wipe is as breathable as the commercial mask. The packing density of gauze is so low that no detectable pressure drop was obtained.

Fig. S2 demonstrates the optical microscopic images in transmission mode for fabrics used in this work. The fibers remained randomly distributed before and after coating with polyaniline. The gauze showed a lower fiber packing density compared to the lint-free wipe. The packing density of the two fabrics was measured as the ratio of fiber density to apparent density. Fiber density was obtained by immersing the fabric in water and weighing the water excluded with the density kit on a balance. Apparent density was got by measuring the mass of the fabric with known dimensions. The results were organized in **Table S4**.

Drying stain of droplets. The size of droplet was obtained by measuring the diameter of drying stain on the detector film, which is only reasonable when the drying stain has the similar size to the droplet itself, and when the contact angle is not too large or too small. In **Fig. S3a** and **S3d**, both unmodified and modified droplet have similar contact angles of around 60°. The images were obtained by pipetting a 10-μL model fluid droplet on the detector screen and taking photo with a smartphone (iphone 7 plus). For the image of modified droplet, the pH of the model fluid was adjusted to 1 with addition of phosphoric acid. The modified droplet looked green due to the reflection from the doped polyaniline. The microscopic top view of 2 μL of unmodified and modified droplet before and after drying are shown in **Fig. S3b** and **3c**, **3e** and **3f**, respectively. The drying stain had the same size as the droplet itself did in both situations. The drying stain looks a little bit different from those in **Fig. 5** because the droplet in **Fig. S3** (2 μL) is much larger than droplets from the sprayer.

Image processing. The processes of quantifying the contrast (*i.e.*, degree of modification) of each droplet with Matlab are illustrated in **Fig. 6** in the main text. Before executing the circle finding program, the original optical microscopy image in reflection mode was processed with a series of filters, in the order of grayscale, Gaussian blur, color inversion and binarization. In this process, grayscale reduced the dimension of images from 3 to 1, Gaussian blur worked as a noise reduction filter, color inversion satisfied the default setting of the algorithm, and binarization maximized the gradients of intensities of pixels at the edge of the droplets. After these pretreatments, the circle locating program based on Hough circle transform was executed which yielded the positions and sizes of the droplets. Hough circle transform[6] reduced unwanted features from the background such as the rolling marks in **Fig. S4a**. If the pre-processed image (**Fig. S4b**) is directly

overlapped on images of transmission, artifacts such as those from the rolling tracks of the plastic film will be counted as droplets (**Fig. S4c**). This will lead to a lot of close-to-zero values of the calculated degree of modification, which increases the level of noise in **Fig. 7** and **8**. With Hough circle transformation, droplets were approximated as circles and those high-aspect-ratio artifacts were removed, improving the overall accuracy of recognizing droplets. The droplet outlines were then overlapped on images of transmission to read the green channel intensity inside and outside droplets. For each droplet, the intensities values of pixels surrounding the circle were collected (the range is 5 pixels surrounding the outline of droplet) and the mode value was calculated to represent the brightness of the background. Next intensity values of pixels inside the droplet were collected and the average value of top 50% intensity values was calculated to represent the brightness of the droplet. The intensity values were averaged over the top 50% but not all intensity to avoid picking pixels outside the droplet as the droplet is not a perfect circle. Then degree of modification for this droplet was calculated according to **Eq. 1**. Matlab codes are available upon requests. The number of droplets and images analyzed are summarized in **Table S2**.

Eq. 1 is justified as follows. In the form of emeraldine, polyaniline exhibits green color upon being doped (emeraldine salt) and turns to blue in neutral to basic condition (emeraldine base). This color shift is due to the shift of absorption band. As a droplet lands on polyaniline, it dopes the polyaniline underneath. In transmission mode of optical microscope, the difference of absorbance of light gives the contrast of acidic droplet against the background, which is most obvious when the wavelength of light is in green range (500 to 600 nm) compared to blue and red range. The doped part of polyaniline was approximated as a cylinder with a cross section equaling to the droplet projection, and thickness of x, as illustrated in **Fig. S5**. The difference of light flux between the doped polyaniline and un-doped can be calculated according to Beer-lambert law:

$$\Phi_d^t = \Phi^i \exp(-\mu_{EB}(H - x) - \mu_{ES}x) \quad \textbf{(Eq. S1)}$$

$$\Phi_b^t = \Phi^i \exp(-\mu_{EB}H) \quad \textbf{(Eq. S2)}$$

$$\exp\big(x \cdot (\mu_{EB} - \mu_{ES})\big) = \frac{\phi_d^t}{\Phi_b^t} \quad \textbf{(Eq. S3)}$$

where Φ^t_d is the flux of transmitted light for a pixel inside a droplet, Φ^t_b is the flux of transmitted light for a pixel belonging to the background, Φ^i is the incoming light flux, H is the thickness of the film, x is the thickness of the green emeraldine salt region, and μ_{EB} and μ_{ES} are attenuation coefficients for emeraldine base and emeraldine salt, respectively. The left-hand side of **Eq. S3** is intrinsically determined by the pH of the droplet. The computer does not store the light intensity directly, instead, it is converted to pixel intensity according to:

$$I = C \times \Phi^t + C' \quad \textbf{(Eq. S4)}$$

Where I is the intensity for each pixel (ranging from 0-255), C is a constant determined by exposure time and gain, C' is determined by offset. By setting offset of the camera to zero, we have:

$$\frac{\phi_d^t}{\Phi_b^t} = 1 + \frac{I_d^P - I_b^P}{I_b^P} = 1 + Degree\ of\ modification \quad \textbf{(Eq. S5)}$$

Where I_d^P is the intensity of a pixel inside the droplet, I_b^P is the intensity of a pixel belong to the background. The physical meaning of degree of modification is related to the difference of light absorption band between acidic (under modified droplets) and neutral (background) area of polyaniline. Droplets are made of thousands of pixels, thus statistical values from those pixels were used to calculate degree of modification for one droplet. For pixels inside droplet, those having the top 50% highest intensities were collected and averaged, the value of which was used for I_d in **Eq. 1**. For pixels surrounding the droplets, the mode value was used for I_b.

Filtration efficiency and escaped droplets. Masks belong to the topic of gas phase filtration, where a model based on single fiber efficiency has been established to explain the mechanism of collection[7,8]. The overall efficiency of the filter, E, is related to the single fiber efficiency by

$$E = 1 - \exp\left(-4\varphi \frac{\alpha}{1-\alpha} \frac{z}{\pi d_f}\right) \quad \textbf{(Eq. S6)}$$

Where α is the packing density, z is the thickness of the filter, and d_f is the diameter of the fiber. φ is the single fiber collection efficiency of a fibrous media, defined as the ratio of flux of particles collected to the flux of particles approaching the fiber. It can be expressed as:

$$\varphi = \eta \cdot h \quad \textbf{(Eq. S7)}$$

Where η is the collision efficiency (note not to be mixed with modification efficiency defined in the main text) and h is the adhesion efficiency. η reflects how many of the incoming droplets collide with fibers and it is usually the dominant factor in determining the filtration rate of a filter. η can be evaluated from five mechanisms: interception, inertia impaction, diffusion, sedimentation, and electrostatic force. η is a function of droplet size. For droplets in micrometer scale, larger droplets can be better captured compared to smaller one due to more efficient interception and inertial impaction. For droplets colliding with fiber, they can either stay on the fiber or bounce off, which is represented by adhesion efficiency h. In generally, a higher speed and large particle size tend to decrease the adhesion efficiency[8,9], which is the reason why masks designed for breathing may be less efficient for coughing. With the addition of modulation layer, however, this problem can be largely mitigated as colliding droplets are modified upon contact with the fibers. Type (2) penetration (**Fig. 9**) corresponds to $\eta(1-h)$. Different from type 1, this part of penetration is expected to be modified droplets.

The model does not consider the interaction between fiber-fiber, particle-particle, and particle-fiber interactions. The collected aerosols can detach from the fibers due to those interaction, especially for liquid aerosols as they can slide, coalesce, and grow larger[9,10], which is defined as type (3). Type (3) cannot be easily expressed in the single fiber model as it is a result of interactions in a bulk material. Collected droplets can be observed either as large droplets or even a liquid film bridging neighboring fibers (**Fig. S6**). After spraying to the polyaniline coated gauze and wipe for 1 s, the two cases were observed under optical microscope immediately. For the gauze, individual coalesced droplet hung on a fiber with large contact angle. Captured droplets on the lint-free wipe, however, formed liquid pools covering fibers, which was a result of high capture rate and short distance between fibers. Regardless of how they are captured, they can be reemitted, either immediately or after incubation time, especially at high airflow speeds. In our experiment, the immediately released droplets were observed. In practice, reemission will be more obvious after the mask is used for a while, which is one of the reasons high-grade mask is not recommended for long time use. The chemical modulation layer can significantly reduce the risk caused by re-entrainment.

The quality factor is defined as[11]:

$$Q = -\ln(1-E)/\Delta P \quad \textbf{(Eq. S8)}$$

Where E is the total efficiency, and ΔP is the pressure drop. A high quality factor is important for respiratory filtration as attempts to increase the total efficiency must not sacrifice breathability. From the **Eq. S6**, we know that the total efficiency can be increased by increasing the packing density, thickness, and single fiber efficiency, or decreasing the diameter of fiber. However, increasing the packing density and thickness will inevitably increase the pressure drop and reduce the quality factor. In our work, none of the parameters were significantly changed before and after coating. However, instead of filtration rate, if we consider the total removal rate which includes both captured droplets and escaped but non-infectious droplets, then φ can be replaced with a higher value of φ'. This increase will be reflected in the increase of total removal efficiency. And one can have a higher removal rate and thus a higher quality factor without any increase in pressure drop. The modification efficiency we measured for gauze and lint-free wipe is the experimental result of $(E(\varphi')-E(\varphi))/(1-E(\varphi))$, which increases with increasing packing density and thickness. Although the gauze is slightly thicker, the packing density is much smaller than the lint-free wipe. This explains the higher modification efficiency for wipe compared to the gauze.

Detection of Cu in escaped droplets. Neocuproine (Nc) is usually used as a color indicator for the titration of Cu(I) ion[12,13]. We found that it is fluorescent, and its fluorescence can be quenched by Cu (II) ions both in the aqueous media (**Fig. S7**) and in a solid matrix. In **Fig. S7**, Nc was dissolved in ethanol at a concentration of 25 mg/mL. With an addition of a few mL of 0.1 M $CuSO_4$ solution, fluorescence quenching was readily observed. A UV lamp (c.a. 360 nm) was placed at the right side of the vial in **Fig. S7** as the source of excitation.

To prepare the fluorometric detector film, poly(methyl methacrylate) (PMMA, Mw ~350,000) was dissolved in anisole at a concentration of 10 mg/mL followed by dissolving Nc at a concentration of 25 mg/mL. The solution was spin-coated on a cover glass (2,000 rpm for 1 min). To calibrate the imaging contrast of droplet stains visualized under fluorescence quenching microscopy (FQM) with the concentration of copper ions, droplets with known concentrations of copper ions from 10^{-5} to 10^{-3} M were sprayed onto the film. It is found that droplets start to leave dark stains with obvious contrast when the Cu concentration is larger than 10^{-4} M (**Fig. S8**). Therefore, the droplets leaving those visual dark stains in **Fig. 10** should contain at least higher than 10^{-4} M of Cu^{2+}, which was found to be sufficient to deactivate influenza viruses.[14]

Control experiments simulating inhalation. The experimental setup to simulate inhalation is shown in **Fig. S9**. For "dry air" conditions, ambient air (23 °C, 40% RH) at an airflow speed of 0.2 m/s was pulled through an unused, $CuSO_4$-loaded gauze by a house vacuum. The downstream air was then guided into a tube containing 3 mL of deionized water. The same process was repeated on a pristine gauze. The concentrations of Cu from Cu-loaded gauze and pristine gauze in deionized water were analyzed to be 2.16 ppb and 1.73 ppb by inductively coupled plasma mass spectrometry (ICP-MS).

Additional experiments were carried out to detect any possible release of either copper ions or acids through damp masking layers by highly humid airflows. An ultrasonic humidifier was used to increase the humidity to 99% RH, as indicated by the humidity sensor placed in the upstream chamber. The humid air was drawn through the masking layer, passing through a downstream chamber before going through a 10 mL of deionized water reservoir in a tube. If any copper salts or acids were released to the downstream air, they should be dissolved in the water reservoir. $CuSO_4$- and H_3PO_4-loaded lint-free wipes were tested. They were first dampened with model respiratory fluid by 1 second of spraying. The airflow speeds were measured by a hot wire anemometer placed at the outlet of the downstream chamber without the fabrics. The reservoir in the gas wash tube was analyzed after passing humid air through for a predetermined duration. Cu ions and acids were detected by ICP-MS and a pH meter, respectively. The process was repeated on a pristine unmodified wipe at 6 m/s for 10 min as a control. The results were summarized in **Table S3**.

Color indication and rechargeability. After extensive spraying, the acid loaded on fabrics will be depleted. Depleted region has a darker color compared to acid rich area due to same principle of color change in the detector film. This can be used as an indicator of the level of acids remaining on the layer. Once depleted, acids can be reloaded onto the layer by immersing in acidic solution, which converts the color of the fabric layer back to green (**Fig. S10**). The gauze in the image was first sprayed continuously for 1 min, which depleted the loaded acids and darkened the color. It was then immersed in phosphoric acid solution (pH 1) again for re-doping. After 30 min, the re-doped gauze was rinsed in ethanol. After drying, the color was recovered back to green.

Supplemental References

1. Mittal, R., Ni, R., and Seo, J.-H. (2020). The flow physics of COVID-19. J Fluid Mech *894*, F2.
2. Han, Z.Y., Weng, W.G., and Huang, Q.Y. (2013). Characterizations of particle size distribution of the droplets exhaled by sneeze. J R Soc Interface *10*, 20130560.
3. Bourouiba, L., Dehandschoewercker, E., and Bush, J.W.M. (2014). Violent expiratory events: on coughing and sneezing. J Fluid Mech *745*, 537-563.
4. Gaetke, L.M., and Chow, C.K. (2003). Copper toxicity, oxidative stress, and antioxidant nutrients. Toxicology *189*, 147-163.
5. Fact Sheet for Health Professionals: Copper. https://ods.od.nih.gov/factsheets/Copper-HealthProfessional/ (September 30, 2020).
6. Kimme, C., Ballard, D., and Sklansky, J. (1975). Finding Circles by an Array of Accumulators. Commun ACM *18*, 120-122.
7. Thomas, D., Charvet, A., Bardin-Monnier, N., and Appert-Collin, J.-C. (2017). Aerosol filtration (ISTE Press - Elsevier).
8. Maus, R., and Umhauer, H. (1997). Single fibre collection and adhesion efficiency for biological particles. Part Part Syst Char *14*, 250-256.
9. Gac, J.M., and Gradon, L. (2012). Analytical investigation and numerical modeling of collisions between a droplet and a fiber. J Colloid Interface Sci *369*, 419-425.
10. Zhang, R.F., Liu, B.F., Yang, A.K., Zhu, Y.Y., Liu, C., Zhou, G.M., Sun, J., Hsu, P.C., Zhao, W.T., Lin, D.C.*, et al.* (2018). In Situ Investigation on the Nanoscale Capture and Evolution of Aerosols on Nanofibers. Nano Lett *18*, 1130-1138.
11. Liu, H., Cao, C.Y., Huang, J.Y., Chen, Z., Chen, G.Q., and Lai, Y.K. (2020). Progress on particulate matter filtration technology: basic concepts, advanced materials, and performances Nanoscale *12*, 437-453.
12. Apak, R., Guclu, K., Demirata, B., Ozyurek, M., Celik, S.E., Bektasoglu, B., Berker, K.I., and Ozyurt, D. (2007). Comparative evaluation of various total antioxidant capacity assays applied to phenolic compounds with the CUPRAC assay. Molecules *12*, 1496-1547.
13. Larsen, E.R. (1974). Spectrophotometric Determination of Copper in Fertilizer with Neocuproine. Anal Chem *46*, 1131-1132.
14. Horie, M., Ogawa, H., Yoshida, Y., Yamada, K., Hara, A., Ozawa, K., Matsuda, S., Mizota, C., Tani, M., Yamamoto, Y.*, et al.* (2008). Inactivation and morphological changes of avian influenza virus by copper ions. Archives of Virology *153*, 1467-1472.